

Bound spinon excitations in the spin- $\frac{1}{2}$ anisotropic triangular antiferromagnet $\text{Ca}_3\text{ReO}_5\text{Cl}_2$


Kazuhiro Nawa¹,² Daigorou Hirai¹,² Maiko Kofu,³ Kenji Nakajima,³ Ryo Murasaki,¹ Satoshi Kogane,² Motoi Kimata,⁴ Hiroyuki Nojiri,⁴ Zenji Hiroi,² and Taku J. Sato¹

¹*Institute of Multidisciplinary Research for Advanced Materials, Tohoku University, 2-1-1 Katahira, Sendai 980-8577, Japan*

²*Institute for Solid State Physics, University of Tokyo, Kashiwa, Chiba 277-8581, Japan*

³*Materials and Life Science Division, J-PARC Center, Tokai, Ibaraki 319-1195, Japan*

⁴*Institute for Materials Research, Tohoku University, Aoba-ku, Sendai 980-8577, Japan*

 (Received 30 June 2020; revised 1 October 2020; accepted 2 October 2020; published 23 October 2020)

The spin excitations of the $S = 1/2$ anisotropic triangular antiferromagnet $\text{Ca}_3\text{ReO}_5\text{Cl}_2$ were investigated by inelastic neutron-scattering experiments. The spin excitation spectrum exhibits sharp dispersive modes in addition to a spinonlike continuum. The sharp modes exhibit large and small dispersions along the intrachain (K) and interchain directions (L), respectively, reflecting a one-dimensional character modified by interchain interactions. The dispersion intensity along the interchain direction is enhanced at the wave vectors around $(K, L) = (0.25, \pm 1.0)$ and $(0.75, 0.0)$ (in reciprocal lattice units, r.l.u.). This enhancement is well explained by the formation of bound spinon pairs. These features are reminiscent of the spin excitations observed in the prototypical compound Cs_2CuCl_4 [Coldea, *et al.*, *Phys. Rev. Lett.* **86**, 1335 (2001); *Phys. Rev. B* **68**, 134424 (2003)]. The consistency with the simulated spectrum based on the random-phase approximation is better for $\text{Ca}_3\text{ReO}_5\text{Cl}_2$ than for Cs_2CuCl_4 , indicating that the spin system in the former remains closer to a Tomonaga-Luttinger liquidlike disordered state. In addition, the low-energy modes exhibit a wave-vector shift along the $\pm K$ direction, suggesting that uniform intrachain Dzyaloshinskii-Moriya interactions are more relevant in $\text{Ca}_3\text{ReO}_5\text{Cl}_2$.

DOI: [10.1103/PhysRevResearch.2.043121](https://doi.org/10.1103/PhysRevResearch.2.043121)

I. INTRODUCTION

The search for elementary excitations with fractional quantum numbers is one of the most intriguing topics in condensed matter physics [1–3]. A representative example is the spinon in a spin-1/2 one-dimensional antiferromagnet. Spinons can be interpreted as domainlike excitations carrying spin-1/2 [4] that obey a dispersion relation identical to that of the des Cloizeaux–Pearson (dCP) mode [5]. A single neutron excites a few pairs of spinons, resulting in a continuum above the dCP mode in inelastic neutron-scattering experiments [6–9]. In addition, fractional excitations under magnetic frustration are possible even in antiferromagnets with two- or three-dimensional lattices. For instance, a triangular-lattice antiferromagnet, which exhibits 120° Néel order [10,11], is suggested to be in the crossover region between a classical ordered state and a quantum disordered ground state [12–14]. The spin excitation spectrum can reflect the fractional excitations related to the quantum disordered state. Indeed, continuous excitations extending to an energy six times as large as the nearest-neighbor interaction have been found

in the triangular-lattice antiferromagnet $\text{Ba}_3\text{CoSb}_2\text{O}_8$ [15]. These excitations may be related to fractionalized excitations.

A spin-1/2 anisotropic triangular-lattice antiferromagnet (ATLAF) comprising two types of interactions, J and J' , is the best candidate for finding and understanding fractionalized excitations. A schematic view of an anisotropic triangular lattice is shown in Fig. 1(a). The spin-1/2 ATLAF can be reduced to a decoupled one-dimensional antiferromagnet when J' is zero and becomes an ideal triangular-lattice antiferromagnet when J' is equal to J . In this sense, the spin-1/2 ATLAF offers an approach to constitute a two-dimensional frustrated system starting from a one-dimensional system, for which the ground state and excitations are well understood.

Neutron-scattering experiments on the representative spin-1/2 ATLAF Cs_2CuCl_4 [16–19] have stimulated much discussion on the ground-state and spin excitations in the spin-1/2 ATLAF [20–39]. This compound exhibits an incommensurate spiral order at $T_N = 0.62$ K [16]. J'/J was estimated as 0.3 [19,40,41]. The magnetic order is induced by Dzyaloshinskii-Moriya (DM) interactions [42–44]. Without the DM interactions, a Tomonaga-Luttinger (TL) liquidlike disordered state is expected to be the ground state for this value of J'/J [30–33,35,36]. Signatures of fractionalization have been observed in inelastic neutron-scattering experiments in which the spin excitation spectra exhibited a spinonlike continuum and sharp dispersive modes [16,17]. Initially, the spin excitations were interpreted as being due to a resonating valence bond state [16,17] or a magnon continuum enhanced by noncollinear magnetic order [38,39].

Published by the American Physical Society under the terms of the [Creative Commons Attribution 4.0 International license](https://creativecommons.org/licenses/by/4.0/). Further distribution of this work must maintain attribution to the author(s) and the published article's title, journal citation, and DOI.

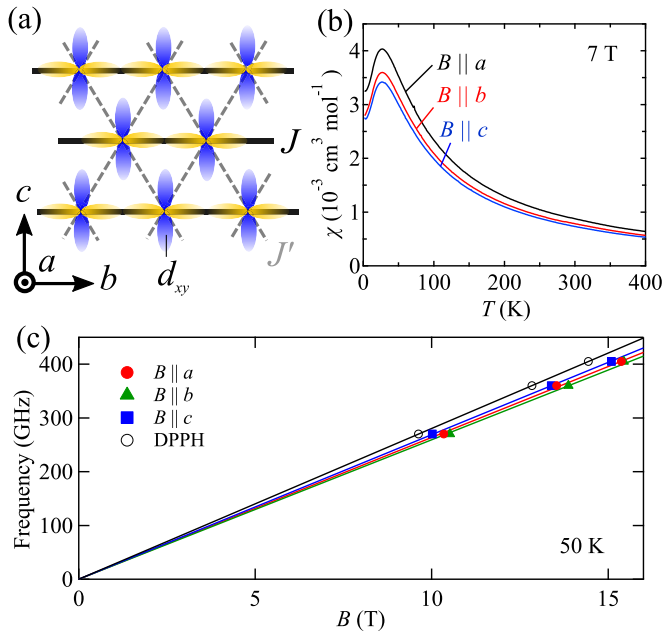


FIG. 1. (a) Schematic view of an anisotropic triangular lattice. The overlap between the Re d_{xy} orbitals leads to the nearest-neighbor and next-nearest-neighbor antiferromagnetic interactions denoted as J and J' , respectively. (b) Temperature dependence of the magnetic susceptibility under magnetic fields of 7 T applied to the a , b , and c axes. (c) Resonance frequencies plotted as functions of the magnetic field. The solid lines correspond to linear fits.

Subsequently, Kohno *et al.* proposed a spinon-based description in which spinons propagate along individual chains and a bound spinon pair propagates between the chains [1,45]. They demonstrated that the spinon-based description can reproduce the spin excitation spectrum without adjustable parameters other than a constant scale factor. The consistency with the experimental results indicates that one-dimensional spin correlations persist over a wide energy range due to the competition between J' in an ATLAF. This description has also been applied to some quasi-one-dimensional antiferromagnets [46]. However, it is not so apparent how long-range order modifies the spinon-based description. Because a spinon bound state is expected to be related to a magnon, which arises from an ordered ground state, it is difficult to distinguish the magnon and spinon excitations from each other in the presence of long-range order.

In consideration of this, the spin-1/2 ATLAF $\text{Ca}_3\text{ReO}_5\text{Cl}_2$ [47,48] should be a better candidate to test the validity of the bound-spinon-pair interpretation in the spinon-based description, because the long-range order is more suppressed in this compound. $\text{Ca}_3\text{ReO}_5\text{Cl}_2$ crystallizes in the orthorhombic space group $Pnma$. Each spin 1/2 is carried by the Re^{6+} ions, which couple with oxygen atoms to form ReO_5 square pyramids. A spin 1/2 occupies the d_{xy} orbital in each square pyramid, forming a spin-1/2 anisotropic triangular lattice on the bc plane [47,48]. Based on the overlap of the d_{xy} orbitals, as shown in Fig. 1(a), the dominant intrachain antiferromagnetic exchange should be along the b direction, while weak interchain exchange may also be present along the c direction. $\text{Ca}_3\text{ReO}_5\text{Cl}_2$ exhibits a magnetic order at $T_N = 1.13$ K, which

is likely to be a DM-induced spiral order, as we discuss later. The magnetic interactions are estimated to be $J = 3.5$ meV and $J'/J = 0.32$ from the temperature dependence of the magnetic susceptibility. This estimate is also supported by density functional theory (DFT) calculations. The ratio $f = J/T_N$ of $\text{Ca}_3\text{ReO}_5\text{Cl}_2$ is almost five times larger than that of Cs_2CuCl_4 . This reduces the influence of magnetic order on the spin excitations in the ATLAF.

In this study we perform single-crystalline magnetization and inelastic neutron-scattering measurements on $\text{Ca}_3\text{ReO}_5\text{Cl}_2$. The paper is organized as follows. The experimental details are described in Sec. II. The magnetization and electron spin resonance (ESR) experiments are presented in Sec. III. Both experiments indicate a small anisotropy in the magnetization and provide evidence that the Re^{6+} ions carry spin 1/2. In Sec. IV we show the spin excitation spectrum, which consists of sharp dispersive modes and a spinon excitation continuum modified by the interchain interactions. The spin excitation spectrum is compared with the simulated spectrum based on the random-phase approximation (RPA) in Sec. V. The wave-vector and energy-transfer region in which the dispersive modes exhibit large intensities matches the region in which a bound spinon pair can appear as a consequence of competing interchain interactions [45]. In Sec. VI, the effect of DM interactions on the low-energy spin excitations in the spin excitation spectrum is discussed. In Sec. VII, the spinon-based description is discussed in terms of the observed spin excitations. The better consistency between the experimental and simulated spectra of $\text{Ca}_3\text{ReO}_5\text{Cl}_2$ compared to Cs_2CuCl_4 indicates that the spin system realized in $\text{Ca}_3\text{ReO}_5\text{Cl}_2$ is closer to a TL liquidlike disordered state. A summary is given in Sec. VIII.

II. EXPERIMENTS

The magnetic susceptibility was measured with a magnetic properties measurement system (Quantum Design). A single crystal grown by the self-flux method [47] was fixed on a quartz sample holder, and a magnetic field of 7 T was applied along the a , b , and c axes. The g value of the paramagnetic state was estimated from the results of high-field ESR experiments using a pulse magnet. A few pieces of single-crystalline samples were coaligned in a sample holder together with a small piece of di(phenyl)-(2,4,6-trinitrophenyl)iminoazanium (DPPH) added as a g marker.

The inelastic neutron-scattering experiments were performed by using the cold-neutron disk chopper spectrometer AMATERAS installed in the Materials and Life Science Experimental Facility at J-PARC, Japan [49]. Thirty single crystals grown by the self-flux method [47] were coaligned on a rectangular Al plate so that the a^* and b^* axes were set on the horizontal scattering plane. The a^* axis was set parallel to the incident neutrons, and the intensities were projected on the b^*-c^* plane. The projection is justified because the dispersion along the a^* direction should be negligible, as expected from the very small overlap of the d_{xy} orbitals [48]. The main data were collected at the incident neutron energies of $E_i = 20.96, 9.71, 5.57,$ and 3.61 meV using repetition multiplication [50]. The monochromating disk choppers were rotated at 300 Hz to achieve energy resolutions of 0.94, 0.28,

0.13, and 0.07 meV, respectively. E_i of 2.63 meV with an energy resolution of 0.04 meV was also used to investigate the low-energy excitations around the magnetic Bragg peak. The sample was cooled down to 0.3 and 2.6 K using a ^3He refrigerator. All the data collected were analyzed using the software suites UTSUSEMI [51] and HORACE [52]. The b -axis length was adjusted to 5.51 Å for the analysis based on the position of the 011 reflection. The effect of the absorption was corrected by regarding the sample as a flat plate with the size of $2.5 \times 2.5 \times 0.1 \text{ cm}^3$ [53,54]. The form factor of Re^{6+} used for the analysis was estimated by performing Fourier transformation on the squared Wannier functions calculated from previous DFT calculation results [48]. The squared Wannier functions describe the electron densities in this system well, because the d_{xy} orbitals are well separated from the other d orbitals.

III. MAGNETIC SUSCEPTIBILITY

The temperature dependence of the magnetic susceptibility is shown in Fig. 1(b). The magnetic susceptibility does not depend significantly on the field direction. This indicates a small magnetization anisotropy. The effective magnetic moment μ_{eff} and Weiss temperature θ are estimated from the Curie-Weiss fits between 100 and 400 K. The fits yield $(\mu_{\text{eff}}, \theta) = [1.647(2) \mu_B, -36.9(2) \text{ K}]$, $[1.568(2) \mu_B, -38.1(3) \text{ K}]$, and $[1.555(1) \mu_B, -41.0(1) \text{ K}]$ for $B \parallel a$, b , and c , respectively. The small difference from the $[1.585(2) \mu_B, -37.8(1) \text{ K}]$ estimated for a polycrystalline sample [48] reflects the anisotropy in the g value. Assuming that Re^{6+} carries spin 1/2, the g values are estimated to be 1.903(2), 1.811(3), 1.796(1), for $B \parallel a$, b , and c , respectively.

The g values estimated from the high-field ESR experiments also suggest the nearly isotropic nature of the exchange interactions. Figure 1(c) shows the linear relations between the frequencies and resonance magnetic fields at 50 K. The resonance magnetic fields are determined by fitting the absorption spectra by Gaussian functions (see the Supplemental Material [55]). From the slopes of the lines, the g values are estimated to be 1.88, 1.85, 1.92 for $B \parallel a$, b , and c , respectively. The g values include an uncertainty of 0.01 due to the broad linewidths of the spectra. These magnitudes are almost consistent with those estimated from the Curie-Weiss fit. The small anisotropy in the g values indicates that the magnetism of this compound should be understood as a spin-1/2 system. In addition, the deviations of the g values from the spin-only value of 2 are small, indicating that there are only small contributions from orbital momentum. For instance, Re^{6+} ions doped in molybdenum oxide exhibit a g value of 1.61–1.67 [56], which is smaller than the 1.85–1.92 of $\text{Ca}_3\text{ReO}_5\text{Cl}_2$. The small deviation from 2 in $\text{Ca}_3\text{ReO}_5\text{Cl}_2$ results from a large crystal-field splitting of 1.4 eV between the $\text{Re } d_{xy}, d_{xz} + d_{yz}$, and $d_{xz} - d_{yz}$ orbitals [47]. Note that a small difference is observed in the g values obtained from the magnetization and ESR measurements for $B \parallel c$. DM interactions might enhance the difference in the magnetic susceptibility at lower fields. The spin excitations observed by inelastic neutron-scattering experiments reflect the existence of the intrachain DM interactions, as discussed in Sec. VI.

IV. SPIN EXCITATION SPECTRUM

Figure 2 shows the intensity maps of the inelastic neutron scattering along K measured at $E_i = 9.71$ and 20.96 meV. Comparing Figs. 2(a)–2(c) measured at 0.3 K and Figs. 2(d)–2(f) measured at 2.6 K, it can be seen that the features of the spin excitations are largely unchanged across the magnetic transition. Thus we first focus on the common features observed in the spin excitations measured at 0.3 and 2.6 K and then discuss the differences between them. As shown in Figs. 2(a)–2(f), a spinonlike continuum with a strong intensity at $K \sim 0.5$ appears across the entire observed L range. A large dispersion along the K direction indicates that the dominant antiferromagnetic exchanges are along the b direction. The lower energy boundaries of the continuum are roughly consistent with the K dependence of the dCP mode, as expected in a spin-1/2 one-dimensional antiferromagnet [5]. Figures 3(a)–3(c) present the intensities integrated across the reciprocal K ranges of $K = [0.20, 0.30]$, $[0.70, 0.80]$, and $[0.45, 0.55]$ (or $[0.48, 0.52]$ for those measured at $E_i = 3.61$ meV), respectively. For the K ranges of $[0.20, 0.30]$ and $[0.70, 0.80]$, the integrated intensities exhibit broad peaks at 5.5–5.7 meV. Assuming that the peak positions correspond to the maximum energy of the dCP mode, $J\pi/2$, the dominant intrachain exchange is estimated to be 3.5–3.6 meV. The magnitude of this rough estimate is consistent with the 3.5 meV estimated from the temperature dependence of the magnetic susceptibility [48]. The small peaks at 7–8 meV in Figs. 3(a) and 3(b) are due to phonons, because strong intensities are indeed observed at large H values beyond the ranges shown in Figs. 2 and 4.

In addition, the intensities against the energy transfer at $K \sim 0.5$ follow the $1/\omega$ dependence expected in a spin-1/2 one-dimensional antiferromagnet. Figure 3(c) shows a semilogarithmic plot in which the intensities measured at a few values of E_i are plotted as functions of the energy transfer. The intensities measured at $E_i = 20.96$ and 3.61 meV are multiplied by a constant scale factor to correct for the incident neutron flux so that the integrated intensities at the elastic position match at $E_i = 9.71$ meV. The intensities are then divided by the magnetic form factor of Re^{6+} . This procedure is necessary because the H component is also increased with increasing energy transfer as a result of the projection along the a^* axis. The dashed curve indicates the $1/\omega$ dependence proposed by Müller [57,58]. The dashed curve agrees with the integrated intensities, indicating the one-dimensional character of the magnetism.

On the other hand, the spin excitations also exhibit unique features that cannot be explained by a spin-1/2 decoupled one-dimensional antiferromagnet. First, the spin excitation spectrum is weakly asymmetric about $K = 0.5$, as shown in Figs. 2(a) and 2(d). The asymmetry is apparent in the integrated intensities shown in Figs. 3(a) and 3(b). The peak energy is larger at $K = [0.20, 0.30]$ than at $K = [0.70, 0.80]$. The difference of 0.2 meV in the peak energy is much larger than the possible shift caused by the magnetic form factor, which strongly reduces the intensity at large wave vectors. The asymmetry depends on the L range used for the integration, as shown in Figs. 2(b), 2(c) 2(e), and 2(f).

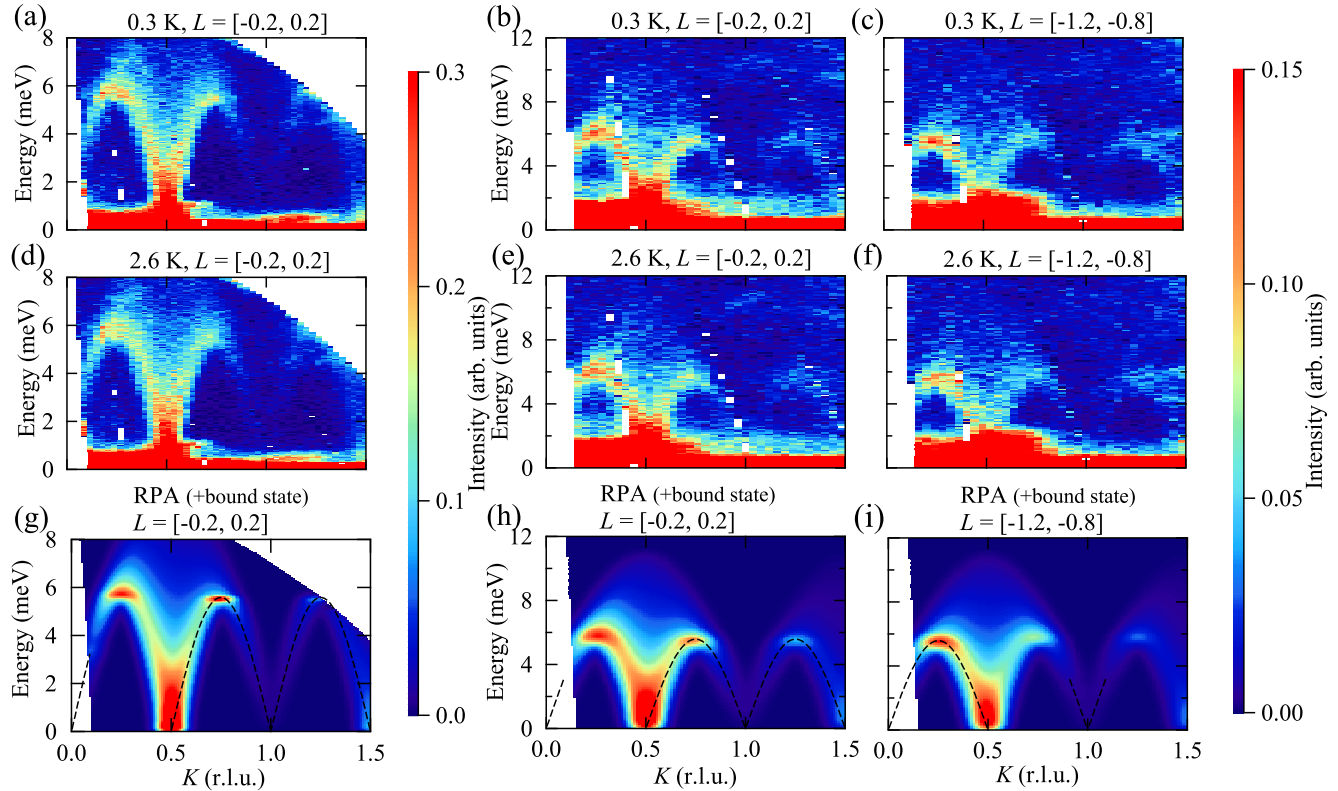


FIG. 2. Color contour maps of scattering intensities along the K direction measured at (a)–(c) 0.3 K and (d)–(f) 2.6 K. The intensity is integrated for the H range below 4.0 r.l.u. (reciprocal lattice unit), and the L range is indicated above each figure. The spectra were collected at (a), (d) $E_i = 9.71$ and (b), (c), (e), (f) 20.96 meV. The intensities from the elastic signals appear as the background below (a), (d) 1 meV and (b), (c), (e), (f) 2 meV. (g)–(i) Color contour maps of scattering intensities simulated by applying the RPA to antiferromagnetically coupled spin-1/2 chains. Each spectrum includes the contribution of dispersive modes from an antibound/bound spinon pair, which are indicated by the black dashed curves.

Second, a small dispersion is present along the L direction, indicating the presence of weak interchain couplings along the c axis. Figure 4 shows the intensity maps along the L direction. The maximum of the lower energy boundaries of the continuum occurs near $L = 0$ for $K = [0.20, 0.30]$, while the minimum occurs near $L = 0$ for $K = [0.70, 0.80]$. This reversed dispersion indicates that the interchain couplings J' are formed along a diagonal direction. The dispersion can also be confirmed from the integrated intensities shown in Figs. 5(a) and 5(b). The peak position shifts to lower energies with decreasing L at $K = [0.20, 0.30]$ [Fig. 5(a)] but shifts to higher energies with decreasing L at $K = [0.70, 0.80]$. The above two features are also observed in the spin excitation spectrum of Cs_2CuCl_4 . This provides evidence for the significance of interchain couplings in the anisotropic triangular lattice of $\text{Ca}_3\text{ReO}_5\text{Cl}_2$.

While the intensities of the continuum are almost temperature independent, the intensities of the dispersive modes increase as the temperature is lowered to 0.3 K. For instance, in the dispersion for the K range of $[0.20, 0.30]$, a sharp dispersion becomes prominent at the L ranges of $[-1.0, -0.5]$ and $[0.5, 1.0]$, as indicated by Figs. 4(a) and 4(e). An intensity increase at 0.3 K is also observed in the K range of $[0.70, 0.80]$. However, the increase occurs at a different L range of

$[-0.5, 0.5]$. The differences between the spin excitation at 0.3 and 2.6 K are also evident in the integrated intensities shown in Figs. 5(a) and 5(b). These differences suggest the coexistence of spin-1 excitations, which propagate between antiferromagnetic chains in addition to the spinon continuum at 0.3 K. For a fixed K , the dispersion intensities increase at the L range where the lower energy boundaries of the continuum become small. This suggests that interchain interactions are relevant for the formation of spin-1 excitations, as we discuss in Sec. V.

V. RPA CALCULATIONS

Because the spin excitations reflect a one-dimensional character, the excitations should be interpreted as spinons or their pairs. Indeed, Kohno *et al.* proposed that incoherent continuum and sharp dispersive modes, such as those observed in Cs_2CuCl_4 , can coexist in an ATAF [45]. The continuum is induced by spinons propagating along each one-dimensional chain, while the dispersive modes are derived from a bound spinon pair. A single spinon cannot propagate between chains because of the competition between interchain interactions. On the other hand, the propagation of a pair of spinons is still possible and leads to a gain in the kinetic energy [1,45].

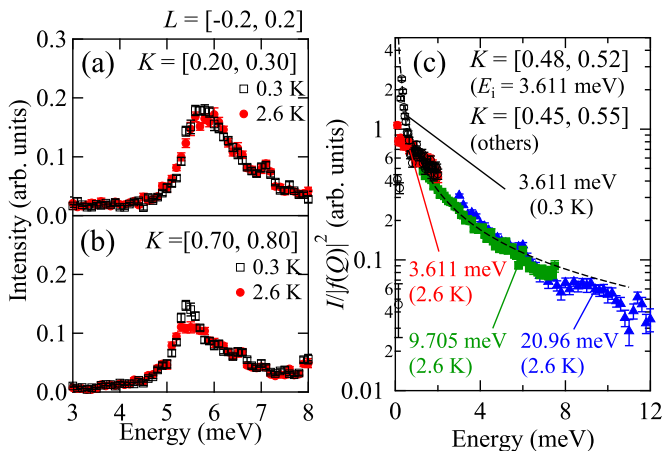


FIG. 3. (a), (b) Integrated intensities plotted against energy at (a) $K = [0.20, 0.30]$ and $L = [-0.2, 0.2]$ and (b) $K = [0.70, 0.80]$ and $L = [-0.2, 0.2]$ measured at $E_i = 9.71$ meV. (c) Integrated intensities plotted against energy at $K \sim 0.50$. Before integration, the intensities are normalized by the integrated intensities at the elastic position and then divided by the Re^{6+} form factor. The data collected at the E_i values of 3.61, 9.71, and 20.96 meV are plotted with the integration ranges of $K = [0.48, 0.52]$ and $L = [-0.6, 0.4]$, $K = [0.45, 0.55]$ and $L = [-0.6, 0.4]$, and $K = [0.45, 0.55]$ and $L = [-1.2, 0.8]$, respectively. The dashed curve represents a $1/\omega$ dependence.

Kohno *et al.* derived a dynamic structure factor by constructing effective Schrödinger equations and then solving them numerically [45]. The dynamical structure factor calculated by their method has almost the same functional form as that derived from the RPA [59,60]. Thus in this study, the spin excitation spectrum is compared with that simulated by applying the RPA to the dynamical susceptibility of a spin $1/2$, weakly coupled one-dimensional antiferromagnet. Here we introduce k_x and k_y as the wave vectors along the intrachain (b^*) and interchain (c^*) directions, respectively. We first calculate the two-spinon contributions to the dynamical structure factor of a one-dimensional chain, $S_{\text{1D}}(k_x, \omega)$, following the analytic procedure presented in Refs. [61] and [62]. The dynamic susceptibility is then derived using the fluctuation-dissipation theorem in the zero-temperature limit and the Kramers-Kronig relation as follows:

$$\text{Im}\chi_{\text{1D}}(k_x, \omega) = \pi \text{sgn}(\omega) S_{\text{1D}}(k_x, |\omega|), \quad (1)$$

$$\text{Re}\chi_{\text{1D}}(k_x, \omega) = \frac{1}{\pi} P \int_{-\infty}^{\infty} d\omega' \frac{\text{Im}\chi_{\text{1D}}(k_x, \omega')}{\omega' - \omega}, \quad (2)$$

where P represents the principal integral. The integration is performed numerically using an adaptive quadrature algorithm. Next, the RPA is applied to the dynamic susceptibility $\chi_{\text{1D}}(k_x, \omega)$, leading to

$$\chi_{\text{RPA}}(k_x, k_y, \omega) = \frac{\chi_{\text{1D}}(k_x, \omega)}{1 + J'(k_x, k_y)\chi_{\text{1D}}(k_x, \omega)}, \quad (3)$$

$$S_{\text{RPA}}(k_x, k_y, \omega) = \frac{1}{\pi} \text{Im}\chi_{\text{RPA}}(k_x, k_y, \omega) \quad (\omega > 0), \quad (4)$$

where $J'(k_x, k_y)$ represents the Fourier transform of the interchain couplings. In addition, the intensities from the spinon

bound state are also considered in the simulation. The dispersion of the spinon bound state $E_{\text{bs}}(\omega)$ is determined by the condition that the denominator of Eq. (4) becomes zero, i.e., $1 + J'(k_x, k_y)\text{Re}\chi_{\text{1D}}(k_x, E_{\text{bs}}) = 0$. Its intensity is given by

$$S_{\text{bs}}(k_x, k_y, \omega) = \delta(\omega - E_{\text{bs}}) \times \left\{ J'(k_x, k_y)^2 \int_0^{\infty} d\omega' \frac{S_{\text{1D}}(k_x, \omega')}{(E_{\text{bs}} - \omega')^2} \right\}^{-1}, \quad (5)$$

which is derived from the wave-function normalization condition. The continuum and sharp dispersive modes correspond to S_{RPA} and S_{bs} , respectively. The calculated intensities are finally multiplied by the form factor of Re^{6+} and convoluted with the Gaussian function to account for the instrument resolution. The wave vector and energy resolutions are estimated by the analytic method [63]. Note that a Gaussian function with an increased linewidth is used for the wave-vector convolution, as we discuss in Sec. VI.

Let us compare the experimental spectra with the simulated dynamical structure factors, which are shown in the color contour maps in Figs. 2(g)–2(i) and 4(i)–4(l). The parameters $J = 3.59$ meV, $J'/J = 0.15$, and a common-scale factor are selected to reproduce the experimental spectra. The estimate of J'/J includes an uncertainty of ± 0.05 because of the incomplete agreement with the experimental data, as discussed below. The simulated spectra reflect the asymmetry of the dispersion against K [Figs. 2(g)–2(i)] and the small dispersion along L [Figs. 4(i)–4(l)] observed in the experiments. The asymmetry and dispersion are induced from the bound state (S_{bs}), whose dispersion is indicated by the black dashed curves in Figs. 2(g)–2(i) and 4(i)–4(l). For instance, as shown in Fig. 2(g), a dispersive mode with large intensities only appears at the K range between 0.5 and 1.5 r.l.u. (reciprocal lattice unit). This results in the difference in the peak position below 0.5 and above 0.5 r.l.u., as shown in Figs. 3(a) and 3(b). In Figs. 5(a) and 5(b), constant wave-vector cuts obtained from the experimental results are compared with those simulated by the decoupled and coupled antiferromagnetic chain models represented by blue dashed and black solid curves, respectively. The blue dashed curves do not reproduce the peak shift. On the other hand, although the agreement is still imperfect, the black solid curves reproduce the line shapes of the integrated intensities measured at 0.3 K better. The broad line shapes at $K = [0.20, 0.30]$ and $L = [-0.2, 0.2]$ correspond to the spinon excitation continuum modified by interchain interactions, while the peak with a tail extending to high energies at $K = [0.70, 0.80]$ and $L = [-0.2, 0.2]$ consists of the sum of the modified continuum and a sharp mode originating from a bound spinon pair. The contributions from the bound spinon pair are necessary to reproduce the entire line shape. Note that weak but finite intensities are also expected from an antibound spinon pair induced by repulsion between spinons. The dispersion of the antibound spinon pair is indicated by the black dashed curves in Figs. 2(g)–2(i). Although the intensities due to the antibound spinon pair can appear at some wave vectors near $(K, L) \sim (0, 0)$ and $(1, -1)$, they were not observed in our experiments because of their small magnitudes.

As we have discussed, the intensity difference between 0.3 and 2.6 K becomes large at certain wave-vector and energy ranges. It should be noted that these wave-vector and energy

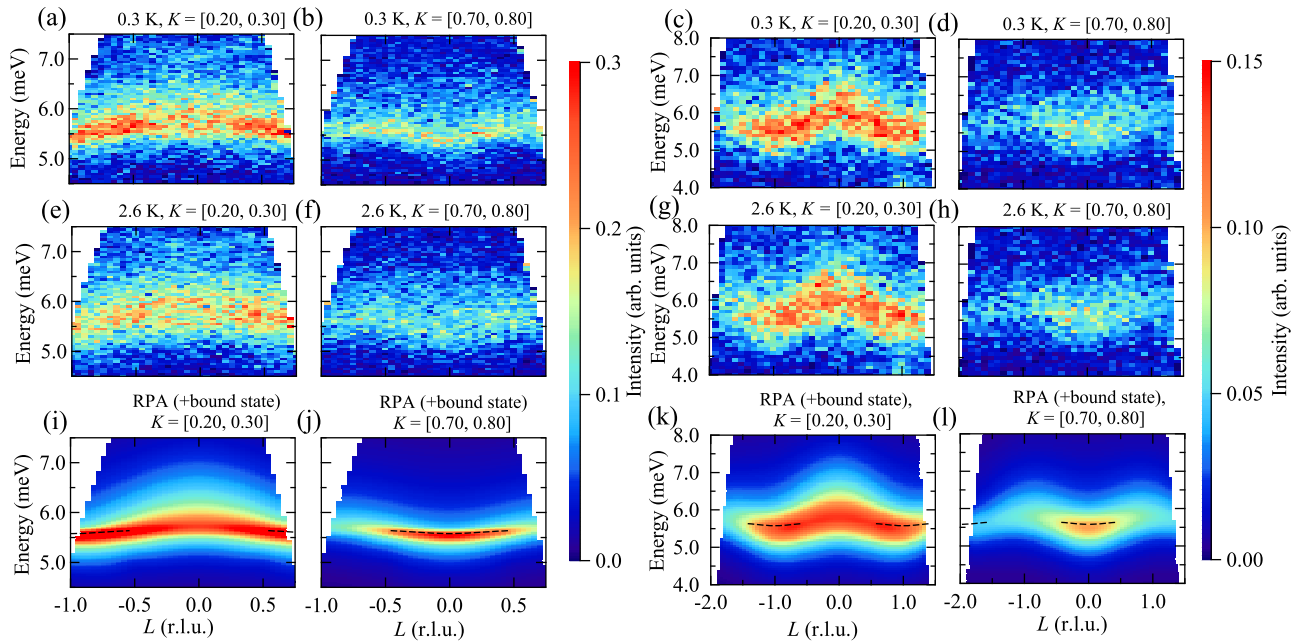


FIG. 4. Color contour maps of scattering intensities along the L direction measured at (a)–(d) 0.3 K and (e)–(h) 2.6 K. The intensity is integrated for the H range below 4.0 r.l.u. and the K range indicated above each figure. The spectra were collected at (a), (b), (e), (f) $E_i = 9.71$ and (c), (d), (g), (h) 20.96 meV. (i)–(l) Color contour maps of scattering intensities simulated by applying the RPA to antiferromagnetically coupled spin-1/2 chains. The dispersive modes from bound spinon pairs are indicated by the black dashed curves.

ranges correspond to the ranges in which dispersive modes from a bound spinon pair are expected. As can be seen in Figs. 4(a), 4(b), 4(e), and 4(f), the intensities are increased at low temperatures at $(K, L) \sim ([0.20, 0.30], [-1.0, -0.5])$, $([0.20, 0.30], [0.5, 1.0])$, and $([0.70, 0.80], [-0.5, 0.5])$. This wave-vector range matches the ranges indicated by the dashed curves in Figs. 4(i) and 4(j). The temperature variation of the integrated intensities is also apparent in Figs. 5(a) and 5(b). A sharp peak emerges at 0.3 K at a peak position consistent with that indicated by the black solid curves. This correspondence suggests that the intensities from the bound spinon pair become prominent as the temperature is decreased down to 0.3 K. This is reasonable because the maximum binding energy to separate the spinon pair is estimated as approximately 0.06 meV (corresponding to 0.7 K), assuming $J = 3.59$ meV and $J'/J = 0.15$.

VI. EFFECT OF DM INTERACTIONS

As described in Secs. IV and V, the excitations above a few meV can be understood as a consequence of the competition between J and J' . On the other hand, those below a few meV cannot be simply explained by only these interactions. Figures 6(a) and 6(b) present a contour map of inelastic neutron scattering measured at 0.3 K and their integrated intensities across certain energy ranges, respectively. Three dispersive modes with almost the same curve shape are observed. One mode exhibits an energy minimum at 0.50 r.l.u. whereas the other two modes are shifted by ± 0.035 r.l.u. along the K direction. The left mode evolves from the magnetic Bragg peak, whose position and intensity are indicated in Fig. 6(f). These features are also corroborated by the contour map in Fig. 6(e). On the other hand, the middle and right modes

exhibit a small energy gap of ~ 0.2 meV. The modes shifted on both sides of 0.50 r.l.u. cannot be reproduced by spin waves with spiral order driven by the competition between J and J' (the dispersion relation of the leading and secondary modes derived from spin-wave theory is given in Ref. [18], for instance). At 2.6 K smeared modes still remain, as shown in Figs. 6(c) and 6(d). The constant-energy cut exhibits a broad peak, which has a much larger FWHM than the resolution of 0.025 r.l.u. Thus, the shift along the K direction should still be present at 2.6 K.

The incommensurate magnetic order and associated wave-vector shift of the low-energy excitations can be induced by interactions between distant sites, such as intrachain next-nearest-neighbor interactions or uniform intrachain DM interactions. The former is unlikely because the magnetic ions are far part: the next-nearest neighbors along the chain are separated by a distance of 11.13 Å, for instance. On the other hand, the latter is more likely because it is allowed by the translational symmetry in $\text{Ca}_3\text{ReO}_5\text{Cl}_2$. The uniform DM terms can be removed by a gauge transformation corresponding to a position-dependent rotation around a DM vector. Thus, for spinon excitations, uniform DM interactions split a degenerate transverse mode into two modes located on both sides of a longitudinal mode in the excitation spectrum. The magnitude of the shift is $\Delta q \sim D/(Jd)$ (d is distance between nearest neighbors) [64–66]. This is the reason for the broadening of the magnetic excitations along the K direction at 2.6 K. On the other hand, it is difficult to interpret the magnetic excitations at 0.3 K because the magnetic structure has not been determined so far. However, because the left and the right modes are shifted from 0.50 r.l.u. in opposite directions by the same magnitude, the intrachain DM interactions are decisive for the magnetic order and associated

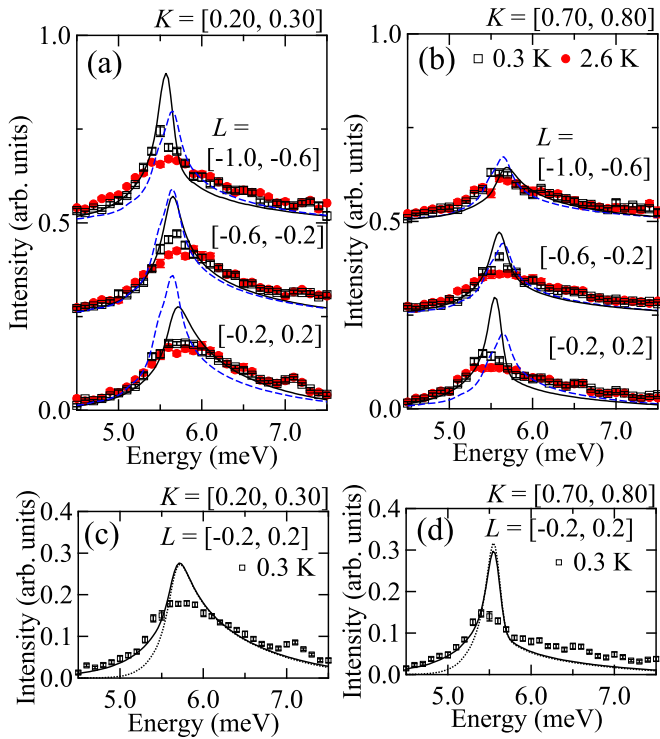


FIG. 5. Integrated intensities plotted against energy at the selected wave-vector ranges of (a) $K = [0.20, 0.30]$ and $L = [-0.2, 0.2]$, $[-0.6, -0.2]$, and $[-1.0, -0.6]$; (b) $K = [0.70, 0.80]$ and $L = [-0.2, 0.2]$, $[-0.6, -0.2]$, and $[-1.0, -0.6]$; (c) $K = [0.20, 0.30]$ and $L = [-0.2, 0.2]$; and (d) $K = [0.70, 0.80]$ and $L = [-0.2, 0.2]$. In (a), (b), the intensities for $L = [-0.6, -0.2]$ and $[-1.0, -0.6]$ are shifted for clarity. The simulated intensities for the coupled and decoupled chains are represented by the black solid and blue dashed curves, respectively. In (c), (d), RPA-based simulated curves with wave-vector convolution performed using a narrower linewidth Gaussian function are plotted as the dotted lines, while the solid lines indicate the same curves convolved with a broader linewidth Gaussian (see text for details).

excitations. For instance, uniform DM interactions can induce a DM-induced spiral order in a spin-1/2 one-dimensional antiferromagnet in which the spiral plane is formed perpendicular to the DM vector. Spin-wave theory predicts that the primary out-of-plane polarized mode can exhibit the minimum energy at $q = \pi/d$. Simultaneously, a gauge transformation into the unrotated frame induces the shift of $\Delta q \sim \pm D/(Jd)$ from $q = \pi/d$ in the in-plane polarized modes [67] due to the high-order spin-wave terms. The magnitude of the energy gap for each mode would be modified by the J' and interchain DM interactions. Thus the shift from 0.50 r.l.u. should be related to uniform DM interactions, regardless of whether the magnetic excitations are interpreted as spinons or magnons.

Note that the above discussion requires the wave-vector shifts to persist up to high energies. Because the wave-vector shift becomes smaller than the wave-vector resolution at large E_i s, the linewidth along the K direction is effectively increased. Indeed, the experimental spectrum reflects the effect of the broadening, as compared in Figs. 5(c) and 5(d). The black dotted and solid curves represent constant wave-

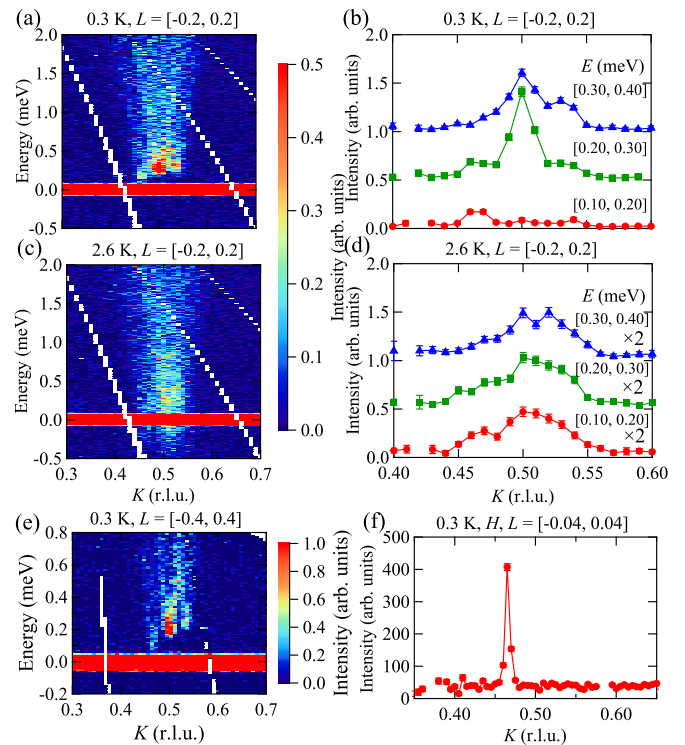


FIG. 6. (a) Color contour map of scattering intensities along the K direction measured at 0.3 K. The intensity is integrated across the L range indicated above the figure. The spectrum was collected at $E_i = 3.61$ meV. (b) Integrated intensities at selected energy ranges plotted as functions of K . The plots obtained by integrating over $[0.20, 0.30]$ and $[0.30, 0.40]$ meV are shifted for clarity. (c), (d) The same contour map and plot as (a), (b) at 2.6 K. (e) The same contour map as (a) measured at $E_i = 2.634$ meV and 0.3 K by rotating the single crystals by 5 degrees around the $(0, 0.50, 0)$ position. (f) Integrated intensities integrated over ± 0.04 meV at the elastic position. The H and L ranges used for the integration are indicated above the figure.

vector cuts of the simulated spectra convoluted by Gaussian functions with different linewidths: the linewidth along K is set equal to the instrument resolution (roughly 0.06 r.l.u. in FWHM) in the former, while it is increased by 0.03×2 r.l.u. for the latter. The convolution using the latter Gaussian function is necessary to reproduce the intensity decrease between 4.5 and 5.5 meV. This suggests that the wave-vector shift is also extended to high energies. The spin excitations between 4.5 and 5.5 meV have a small difference between 0.3 and 2.6 K, suggesting that the wave-vector shift at high energies is preserved even above T_N .

The wave-vector shift in magnon branches induced by DM interactions has often been observed in neutron-scattering experiments. In particular, an incommensurate spiral order often induces a wave-vector shift of the magnons, as we have discussed so far. Another example is α - $\text{Cu}_2\text{V}_2\text{O}_7$, which exhibits a commensurate collinear antiferromagnetic order [68]. The uniform DM component parallel to the magnetic moment shifts the minimum of the magnon branches to the incommensurate wave-vector position [69]. Although $\text{Ca}_3\text{ReO}_5\text{Cl}_2$ exhibits incommensurate order at low temperatures, the spin

excitation spectrum suggests that the wave-vector shift also applies to spinon excitations. Uniform DM interactions can induce the wave-vector shift of spinon excitations through the action of the Rashba-type spin-orbit interaction on the electrons. This was first observed in the field dependence of the resonance frequency in ESR measurements on Cs_2CuCl_4 [66]. While the ESR measurements have focused on the wave-vector range near $q = 0$, our observation suggests a wave-vector shift over a broad wave-vector range.

We finally make short comments on the possible magnetic structure. Only a single magnetic Bragg peak at $(0, 0.465, 0)$ was detected because of the reduced moment size and strongly decaying form factor of Re^{6+} . As previously discussed for Cs_2CuCl_4 , the intrachain and interchain DM interactions would lead to a DM-induced spiral phase [42,43]. Even weak interchain DM interactions can become more relevant than J' because they are staggered along the chain and thus do not compete with antiferromagnetic J [42,43]. The same argument can also be applied to $\text{Ca}_3\text{ReO}_5\text{Cl}_2$, in which the crystal symmetry imposes the same constraints on exchange interactions as those in Cs_2CuCl_4 . Thus intrachain DM interactions as well as interchain DM interactions may also stabilize the DM-induced spiral order in $\text{Ca}_3\text{ReO}_5\text{Cl}_2$. The detailed magnetic structure will be determined in further neutron-diffraction experiments.

VII. DISCUSSION

The comparison between the experimental and simulated spectra indicates that spin excitations in the ATLAF $\text{Ca}_3\text{ReO}_5\text{Cl}_2$ are dominated by spinons. The major features of the spin excitations are largely unchanged across the magnetic transition. In addition, at 0.3 K, a sharp dispersive mode develops at certain wave vectors and energy transfers from which bound spinon pairs should emerge. This provides evidence for the formation of a bound spinon pair. The intensities would be better reproduced by introducing interactions between bound spinon pairs, which have not been considered in the simulation. J'/J is estimated to be 0.15, which is almost half of the 0.32 estimated by fitting the temperature dependence of the magnetic susceptibility [48]. The discrepancy may be due to DM interactions, which have not been explicitly included in our simulation. The intrachain DM interactions split the dispersive mode along the K direction, and the interchain DM interactions directly modify the dispersion along the L direction [64]. These interactions make it difficult to estimate J'/J precisely. In addition, the values of J'/J estimated from the magnetic susceptibility and the spin excitation spectrum also include uncertainties of ± 0.1 and ± 0.05 , respectively, due to adjustable parameters that can affect one another other.

A disadvantage of the spinon-based description is that the effects of the magnetic order are neglected, whereas $\text{Ca}_3\text{ReO}_5\text{Cl}_2$ exhibits magnetic order at 1.13 K [48]. Theoretical studies have predicted that the ground state should be a TL liquidlike disordered state in the range of $J'/J < 0.5$ [30–33,35,36]. However, in reality, intrachain and interchain DM interactions can induce a spiral order [42–44]. Simultaneously, the DM interactions would also destabilize the bound spinon pair. If the interchain coupling is not very strong,

the dynamical structure factor can be well approximated by applying the RPA to that of each chain defined in the unrotated frame. Thus, under uniform DM interactions that yield a wave-vector shift of Δq , the dispersive mode of a bound spinon pair extends to negative energy near $q = \pi/a + \Delta q$. This indicates that an instability develops at this wave vector [64]. In other words, at least in the low-energy range, spin excitations should be interpreted as magnons due to the long-range order rather than a bound spinon pair. On the other hand, for high-energy excitations, the consistency between the line shapes of the simulated and experimental spectra indicates that the spinon-based description is still applicable. This suggests that $\text{Ca}_3\text{ReO}_5\text{Cl}_2$ should be near the crossover region between a classical ordered state and a TL liquidlike disordered ground state. The existence of a crossover energy above which the spinon-based description can be well applied can be naturally deduced by analogy to quasi-one-dimensional antiferromagnets. For instance, spin excitations above the crossover energy follow the energy-temperature scaling for a TL liquid even if the temperature is much lower than T_N in KCuF_3 [9]. For $\text{Ca}_3\text{ReO}_5\text{Cl}_2$, although the same scaling cannot be applied because of the intrachain DM interactions, a crossover energy would exist at roughly 1 meV. Below this energy, sharp dispersive modes corresponding to magnons become apparent at 0.3 K, while above this energy, the spin excitations are well described in terms of a TL liquidlike disordered state irrespective of the temperature. Note that the DM interactions should not modify the dynamical structure factor substantially at high energies as long as the interchain coupling is sufficiently weak and the RPA calculations are applicable.

The effect of long-range order can be discussed by comparing the spin excitation spectra of $\text{Ca}_3\text{ReO}_5\text{Cl}_2$ and Cs_2CuCl_4 [17,18]. In Cs_2CuCl_4 , a constant-wave-vector cut shows a double-peak structure even at a wave vector where a bound spinon pair should not be present (A–D scan in Refs. [17] and [18] and F scan in Ref. [18]). This differs from $\text{Ca}_3\text{ReO}_5\text{Cl}_2$, which only exhibits the broad continuum shown in Figs. 3 and 5. In addition, the integrated intensities from the bound spinon pair are much stronger in Cs_2CuCl_4 (E scan in Ref. [18]) than those from the modified continuum. Thus the magnetic order would enhance the intensities of some dispersive modes, some of which are interpreted as a bound state in spinon language. This effect is prominent in Cs_2CuCl_4 , while the spinon-based description fits the spin excitation spectrum of $\text{Ca}_3\text{ReO}_5\text{Cl}_2$ better. The spin system realized in $\text{Ca}_3\text{ReO}_5\text{Cl}_2$ should be closer to a TL liquidlike disordered state than the spin system in Cs_2CuCl_4 .

The ground state and associated spin excitations are affected by a few factors: J' , interplane interactions J'' , and DM interactions. From the spin excitation spectrum, J'/J in $\text{Ca}_3\text{ReO}_5\text{Cl}_2$ is estimated as $J'/J = 0.15$, which is almost half of the 0.3 in Cs_2CuCl_4 [19,40,41]. J''/J should be very small according to the DFT calculations, which yielded a J''/J smaller than 0.001 [48]. The small J' and J'' may be the reason why the spin system in $\text{Ca}_3\text{ReO}_5\text{Cl}_2$ is close to the TL liquidlike disordered state and the intensities from the bound spinon pair are thus weaker in $\text{Ca}_3\text{ReO}_5\text{Cl}_2$ than in Cs_2CuCl_4 . A rough estimate of the DM interactions can be made from the wave-vector shift of the magnetic Bragg

peak from the (0, 0.50, 0) position under the assumption that intrachain DM interactions dominate the incommensurate magnetic order rather than J' . The shift of 0.035 r.l.u. in $\text{Ca}_3\text{ReO}_5\text{Cl}_2$ is larger than the 0.028 r.l.u. in Cs_2CuCl_4 [16], suggesting that the DM interactions would be stronger. This is reasonable because the spin-orbit coupling is stronger in Re atoms than in Cu atoms. To reveal the relation between magnons due to DM interactions and the bound spinon pair, the magnetic structure would need to be clarified. In addition, it is interesting to investigate the excitations of an ATLAF without DM interactions, which can be realized under certain crystal symmetries [70]. In the absence of DM interactions, the low-energy spin excitations should reflect the nature of the disordered ground state [23,24].

VIII. SUMMARY

The spin excitations in a spin-1/2 ATLAF $\text{Ca}_3\text{ReO}_5\text{Cl}_2$ were explained using the spinon-based description, reflecting the strong one-dimensional nature of the magnetism in the material. The spectrum can be understood in terms of dispersive modes derived from a bound spinon pair and the spinonlike continuum modified by interchain interactions. The consistency between the experimental and simulated spectra indicates that the spin model realized in $\text{Ca}_3\text{ReO}_5\text{Cl}_2$ is in the vicinity of a TL liquidlike disordered state expected in an

ATLAF with moderate J'/J . In addition, the persistence of the wave-vector shift in the spinon excitations above T_N suggests the presence of effective uniform intrachain DM interactions.

ACKNOWLEDGMENTS

The neutron-scattering experiment was performed under the J-PARC user program (Proposal No. 2018A0044). The x-ray diffraction experiments to confirm the quality of the single-crystalline samples were supported by the Visiting Researcher's Program of the Institute for Solid State Physics, University of Tokyo. We express our sincere gratitude to M. Kawamura for providing the results of the DFT calculations and to I. Zaliznyak, G. J. Nilsen, S. A. Zvyagin, and K. Matan for valuable discussions. This work was supported by Grants-in-Aid for Early-Career Scientists (No. 20K14395), Scientific Research on Innovative Areas (Nos. 19H04688 and 19H05824), Scientific Research (B) (Nos. 19H01834 and 20H01858), Challenging Research (Exploratory) (No. 19K21839), and Fund for the Promotion of the Joint International Research (Fostering Joint International Research) (No. 18KK0150 and No. 19KK0069) from the Japan Society for the Promotion of Science, and the CORE Laboratory Research Program "Dynamic Alliance for Open Innovation Bridging Human, Environment and Materials" of the Network Joint Research Center for Materials and Device.

-
- [1] L. Balents, Spin liquids in frustrated magnets, *Nature (London)* **464**, 199 (2010).
 - [2] A. Vasiliev, O. Volkova, E. Zvereva, and M. Markina, Milestones of low-D quantum magnetism, *npj Quantum Mater.* **3**, 18 (2018).
 - [3] D. A. Tennant, Studies of spinons, Majoranas, and monopoles in spin liquid and quantum critical magnets with neutrons, *J. Phys. Soc. Jpn.* **88**, 081009 (2019).
 - [4] L. Faddeev and L. Takhtajan, What is the spin of a spin wave?, *Phys. Lett. A* **85**, 375 (1981).
 - [5] J. des Cloizeaux and J. J. Pearson, Spin-wave spectrum of the antiferromagnetic linear chain, *Phys. Rev.* **128**, 2131 (1962).
 - [6] Y. Endoh, G. Shirane, R. J. Birgeneau, P. M. Richards, and S. L. Holt, Dynamics of an $S = 1/2$, One-Dimensional Heisenberg Antiferromagnet, *Phys. Rev. Lett.* **32**, 170 (1974).
 - [7] S. E. Nagler, D. A. Tennant, R. A. Cowley, T. G. Perring, and S. K. Satija, Spin dynamics in the quantum antiferromagnetic chain compound KCuF_3 , *Phys. Rev. B* **44**, 12361 (1991).
 - [8] D. A. Tennant, T. G. Perring, R. A. Cowley, and S. E. Nagler, Unbound Spinons in the $S = 1/2$ Antiferromagnetic Chain KCuF_3 , *Phys. Rev. Lett.* **70**, 4003 (1993).
 - [9] B. Lake, D. A. Tennant, C. D. Frost, and S. E. Nagler, Quantum criticality and universal scaling of a quantum antiferromagnet, *Nat. Mater.* **4**, 329 (2005).
 - [10] L. Capriotti, A. E. Trumper, and S. Sorella, Long-Range Néel Order in the Triangular Heisenberg Model, *Phys. Rev. Lett.* **82**, 3899 (1999).
 - [11] S. R. White and A. L. Chernyshev, Néel Order in Square and Triangular Lattice Heisenberg Models, *Phys. Rev. Lett.* **99**, 127004 (2007).
 - [12] A. V. Chubukov, S. Sachdev, and T. Senthil, Quantum phase transitions in frustrated quantum antiferromagnets, *Nucl. Phys. B* **426**, 601 (1994).
 - [13] R. Moessner and S. L. Sondhi, Resonating Valence Bond Phase in the Triangular Lattice Quantum Dimer Model, *Phys. Rev. Lett.* **86**, 1881 (2001).
 - [14] E. A. Ghioldi, M. G. Gonzalez, S. S. Zhang, Y. Kamiya, L. O. Manuel, A. E. Trumper, and C. D. Batista, Dynamical structure factor of the triangular antiferromagnet: Schwinger boson theory beyond mean field, *Phys. Rev. B* **98**, 184403 (2018).
 - [15] S. Ito, N. Kurita, H. Tanaka, S. O. Kawamura, K. Nakajima, S. Itoh, K. Kuwahara, and K. Kakurai, Structure of the magnetic excitations in the spin-1/2 triangular-lattice Heisenberg antiferromagnet $\text{Ba}_3\text{CoSb}_2\text{O}_9$, *Nat. Commun.* **8**, 235 (2017).
 - [16] R. Coldea, D. A. Tennant, R. A. Cowley, D. F. McMorrow, B. Dorner, and Z. Tylczynski, Neutron scattering study of the magnetic structure of Cs_2CuCl_4 , *J. Phys.: Condens. Matter* **8**, 7473 (1996).
 - [17] R. Coldea, D. A. Tennant, A. M. Tsvelik, and Z. Tylczynski, Experimental Realization of a 2D Fractional Quantum Spin Liquid, *Phys. Rev. Lett.* **86**, 1335 (2001).
 - [18] R. Coldea, D. A. Tennant, and Z. Tylczynski, Extended scattering continua characteristic of spin fractionalization in the two-dimensional frustrated quantum magnet Cs_2CuCl_4 observed by neutron scattering, *Phys. Rev. B* **68**, 134424 (2003).
 - [19] R. Coldea, D. A. Tennant, K. Habicht, P. Smeibidl, C. Wolters, and Z. Tylczynski, Direct Measurement of the Spin Hamiltonian and Observation of Condensation of Magnons in the 2D Frustrated Quantum Magnet Cs_2CuCl_4 , *Phys. Rev. Lett.* **88**, 137203 (2002).

- [20] L. O. Manuel and H. A. Ceccatto, Magnetic and quantum disordered phases in triangular-lattice Heisenberg antiferromagnets, *Phys. Rev. B* **60**, 9489 (1999).
- [21] C. H. Chung, K. Voelker, and Y. B. Kim, Large- N solutions of the Heisenberg and Hubbard–Heisenberg models on the anisotropic triangular lattice: Application to Cs_2CuCl_4 and to the layered organic superconductors κ -(BEDT-TTF) $_2$ X (BEDT-TTF \equiv bis(ethylene-dithio)tetrathiafulvalene); X \equiv anion), *J. Phys.: Condens. Matter* **13**, 5159 (2001).
- [22] C. H. Chung, K. Voelker, and Y. B. Kim, Statistics of spinons in the spin-liquid phase of Cs_2CuCl_4 , *Phys. Rev. B* **68**, 094412 (2003).
- [23] J. Alicea, O. I. Motrunich, and M. P. A. Fisher, Algebraic Vortex Liquid in Spin-1/2 Triangular Antiferromagnets: Scenario for Cs_2CuCl_4 , *Phys. Rev. Lett.* **95**, 247203 (2005).
- [24] S. V. Isakov, T. Senthil, and Y. B. Kim, Ordering in Cs_2CuCl_4 : Possibility of a proximate spin liquid, *Phys. Rev. B* **72**, 174417 (2005).
- [25] Y. Hauashi and M. Ogata, Possibility of gapless spin liquid state by one-dimensionalization, *J. Phys. Soc. Jpn.* **76**, 053705 (2007).
- [26] Zheng Weihong, R. H. McKenzie, and R. P. Singh, Phase diagram for a class of spin- $\frac{1}{2}$ Heisenberg models interpolating between the square-lattice, the triangular-lattice, and the linear-chain limits, *Phys. Rev. B* **59**, 14367 (1999).
- [27] W. Zheng, J. O. Fjærestad, R. R. P. Singh, R. H. McKenzie, and R. Coldea, Anomalous Excitation Spectra of Frustrated Quantum Antiferromagnets, *Phys. Rev. Lett.* **96**, 057201 (2006).
- [28] W. Zheng, J. O. Fjærestad, R. R. P. Singh, R. H. McKenzie, and R. Coldea, Excitation spectra of the spin- $\frac{1}{2}$ triangular-lattice Heisenberg antiferromagnet, *Phys. Rev. B* **74**, 224420 (2006).
- [29] S. Yunoki and S. Sorella, Resonating Valence Bond Wave Function for the Two-Dimensional Fractional Spin Liquid, *Phys. Rev. Lett.* **92**, 157003 (2004).
- [30] S. Yunoki and S. Sorella, Two spin liquid phases in the spatially anisotropic triangular Heisenberg model, *Phys. Rev. B* **74**, 014408 (2006).
- [31] D. Heidarian, S. Sorella, and F. Becca, Spin-1/2 Heisenberg model on the anisotropic triangular lattice: From magnetism to a one-dimensional spin liquid, *Phys. Rev. B* **80**, 012404 (2009).
- [32] E. Ghorbani, L. F. Tocchio, and F. Becca, Variational wave functions for the $S = 1/2$ Heisenberg model on the anisotropic triangular lattice: Spin liquids and spiral orders, *Phys. Rev. B* **93**, 085111 (2016).
- [33] M. Q. Weng, D. N. Sheng, Z. Y. Weng, and R. J. Bursill, Excitation spectra of the spin-1/2 triangular-lattice Heisenberg antiferromagnet, *Phys. Rev. B* **74**, 012407 (2006).
- [34] A. Weichselbaum and S. R. White, Incommensurate correlations in the anisotropic triangular Heisenberg lattice, *Phys. Rev. B* **84**, 245130 (2011).
- [35] M. Thesberg and E. S. Sørensen, Exact diagonalization study of the anisotropic triangular lattice Heisenberg model using twisted boundary conditions, *Phys. Rev. B* **90**, 115117 (2014).
- [36] J. Reuther and R. Thomale, Functional renormalization group for the anisotropic triangular antiferromagnet, *Phys. Rev. B* **83**, 024402 (2011).
- [37] K. Harada, Numerical study of incommensurability of the spiral state on spin-1/2 spatially anisotropic triangular antiferromagnets using entanglement renormalization, *Phys. Rev. B* **86**, 184421 (2012).
- [38] M. Y. Veillette, A. J. A. James, and F. H. L. Essler, Spin dynamics of the quasi-two-dimensional spin-1/2 quantum magnet Cs_2CuCl_4 , *Phys. Rev. B* **72**, 134429 (2005).
- [39] D. Dalidovich, R. Sknepnek, A. J. Berlinsky, J. Zhang, and C. Kallin, Spin structure factor of the frustrated quantum magnet Cs_2CuCl_4 , *Phys. Rev. B* **73**, 184403 (2006).
- [40] W. Zheng, R. R. P. Singh, R. H. McKenzie, and R. Coldea, Temperature dependence of the magnetic susceptibility for triangular-lattice antiferromagnets with spatially anisotropic exchange constants, *Phys. Rev. B* **71**, 134422 (2005).
- [41] S. A. Zvyagin, D. Kamenskyi, M. Ozerov, J. Wosnitzer, M. Ikeda, T. Fujita, M. Hagiwara, A. I. Smirnov, T. A. Soldatov, A. Y. Shapiro, J. Krzystek, R. Hu, H. Ryu, C. Petrovic, and M. E. Zhitomirsky, Direct Determination of Exchange Parameters In Cs_2CuBr_4 and Cs_2CuCl_4 : High-Field Electron-Spin-Resonance Studies, *Phys. Rev. Lett.* **112**, 077206 (2014).
- [42] O. A. Starykh and L. Balents, Ordering in Spatially Anisotropic Triangular Antiferromagnets, *Phys. Rev. Lett.* **98**, 077205 (2007).
- [43] O. A. Starykh, H. Katsura, and L. Balents, Extreme sensitivity of a frustrated quantum magnet: Cs_2CuCl_4 , *Phys. Rev. B* **82**, 014421 (2010).
- [44] S. Ghamari, C. Kallin, S.-S. Lee, and E. S. Sørensen, Order in a spatially anisotropic triangular antiferromagnet, *Phys. Rev. B* **84**, 174415 (2011).
- [45] M. Kohno, O. A. Starykh, and L. Balents, Spinons and triplons in spatially anisotropic frustrated antiferromagnets, *Nat. Phys.* **3**, 790 (2007).
- [46] J. C. Leiner, J. Oh, A. I. Kolesnikov, M. B. Stone, M. D. Le, E. P. Kenny, B. J. Powell, M. Mourigal, E. E. Gordon, M.-H. Whangbo, J.-W. Kim, S.-W. Cheong, and J.-G. Park, Magnetic excitations of the Cu^{2+} quantum spin chain in $\text{Sr}_3\text{CuPtO}_6$, *Phys. Rev. B* **97**, 104426 (2018).
- [47] D. Hirai, T. Yajima, D. N. Hamane, C. Kim, H. Akiyama, M. Kawamura, T. Misawa, N. Abe, T. Arima, and Z. Hiroi, “Visible” $5d$ orbital states in a pleochroic oxychloride, *J. Am. Chem. Soc.* **139**, 10784 (2017).
- [48] D. Hirai, K. Nawa, M. Kawamura, T. Misawa, and Z. Hiroi, One-dimensionalization by geometrical frustration in the anisotropic triangular lattice of the $5d$ quantum antiferromagnet $\text{Ca}_3\text{ReO}_5\text{Cl}_2$, *J. Phys. Soc. Jpn.* **88**, 044708 (2019).
- [49] K. Nakajima, S. Ohira-Kawamura, T. Kikuchi, M. Nakamura, R. Kajimoto, Y. Inamura, N. Takahashi, K. Aizawa, K. Suzuya, K. Shibata, T. Nakatani, K. Soyama, R. Maruyama, H. Tanaka, W. Kambara, T. Iwahashi, Y. Itoh, T. Osakabe, S. Wakimoto, K. Kakurai *et al.*, AMATERAS: A cold-neutron disk chopper spectrometer, *J. Phys. Soc. Jpn.* **80**, SB028 (2011).
- [50] M. Nakamura, R. Kajimoto, Y. Inamura, F. Mizuno, and M. Fujita, First demonstration of novel method for inelastic neutron scattering measurement utilizing multiple incident energies, *J. Phys. Soc. Jpn.* **78**, 093002 (2009).
- [51] Y. Inamura, T. Nakatani, J. Suzuki, and T. Otomo, Development status of software “Utsusemi” for chopper spectrometers at MLF, J-PARC, *J. Phys. Soc. Jpn.* **82**, SA031 (2013).
- [52] R. A. Ewings, A. Buts, M. D. Lee, J. van Duijn, I. Bustinduy, and T. Perring, Horace: Software for the analysis of data from single crystal spectroscopy experiments at time-of-flight

- neutron instruments, *Nucl. Instrum. Methods Phys. Res., Sect. A* **834**, 132 (2016).
- [53] H. Kadowaki, M. Wakita, B. Fåk, J. Ollivier, S. Ohira-Kawamura, K. Nakajima, H. Takatsu, and M. Tamai, Continuum excitation and pseudospin wave in quantum spin-liquid and quadrupole ordered states of $Tb_{2+x}Ti_{2-x}O_{7+y}$, *J. Phys. Soc. Jpn.* **87**, 064704 (2018).
- [54] H. Kadowaki, <https://github.com/kadowaki-h/absorptionfactoramateras>.
- [55] See Supplemental Material at <http://link.aps.org/supplemental/10.1103/PhysRevResearch.2.043121> for the estimation of the g value.
- [56] R. Gazzinelli, O. F. Schirmer, and V. Wittwer, ESR and optical absorption of rhenium in MoO_3 , *J. Phys. C: Solid State Phys.* **10**, 889 (1977).
- [57] G. Müller, H. Beck, and J. C. Bonner, Zero-Temperature Dynamics of the $S = 1/2$ Linear Heisenberg Antiferromagnet, *Phys. Rev. Lett.* **43**, 75 (1979).
- [58] G. Müller, H. Thomas, H. Beck, and J. C. Bonner, Quantum spin dynamics of the antiferromagnetic linear chain in zero and nonzero magnetic field, *Phys. Rev. B* **24**, 1429 (1981).
- [59] D. J. Scalapino, Y. Imry, and P. Pincus, Generalized Ginzburg-Landau theory of pseudo-one-dimensional systems, *Phys. Rev. B* **11**, 2042 (1975).
- [60] H. J. Schulz, Dynamics of Coupled Quantum Spin Chains, *Phys. Rev. Lett.* **77**, 2790 (1996).
- [61] A. H. Bougourzi, M. Couture, and M. Kacir, Exact two-spinon dynamical correlation function of the one-dimensional Heisenberg model, *Phys. Rev. B* **54**, R12669(R) (1996).
- [62] M. Karbach, G. Müller, A. H. Bougourzi, A. Fledderjohann, and K. H. Mütter, Two-spinon dynamic structure factor of the one-dimensional $s = 1/2$ Heisenberg antiferromagnet, *Phys. Rev. B* **55**, 12510 (1997).
- [63] R. Kajimoto, K. Sato, Y. Inamura, and M. Fujita, Instrumental resolution of the chopper spectrometer 4SEASONS evaluated by Monte Carlo simulation, in *Proceedings of the Joint Conference on Quasielastic Neutron Scattering and the Workshop on Inelastic Neutron Spectrometers QENS/WINS 2016: Probing Nanoscale Dynamics in Energy Related Materials*, edited by F. Fernandez-Alonso, D. L. Price, V. Grzimek, W. Lohstroh, A. Schneidewind, and M. Russina, AIP Conf. Proc. No. 1969 (AIP, New York, 2018), p. 050004.
- [64] M. Bocquet, F. H. L. Essler, A. M. Tsvelik, and A. O. Gogolin, Finite-temperature dynamical magnetic susceptibility of quasi-one-dimensional frustrated spin-1/2 Heisenberg antiferromagnets, *Phys. Rev. B* **64**, 094425 (2001).
- [65] S. Gangadharaiah, J. Sun, and O. A. Starykh, Spin-orbital effects in magnetized quantum wires and spin chains, *Phys. Rev. B* **78**, 054436 (2008).
- [66] K. Y. Povarov, A. I. Smirnov, O. A. Starykh, S. V. Petrov, and A. Y. Shapiro, Modes of Magnetic Resonance in the Spin-Liquid Phase of Cs_2CuCl_4 , *Phys. Rev. Lett.* **107**, 037204 (2011).
- [67] The wave-vector shift in a spiral order induced by uniform DM interactions is discussed in, for instance, A. Zheludev, S. Maslov, G. Shirane, I. Tsukada, T. Masuda, K. Uchinokura, I. Zaliznyak, R. Erwin, and L. P. Regnault, Magnetic anisotropy and low-energy spin waves in the Dzyaloshinskii-Moriya spiral magnet $Ba_2CuGe_2O_7$, *Phys. Rev. B* **59**, 11432 (1999).
- [68] G. Gitgeatpong, Y. Zhao, M. Avdeev, R. O. Piltz, T. J. Sato, and K. Matan, Magnetic structure and Dzyaloshinskii-Moriya interaction in the $S = 1/2$ helical-honeycomb antiferromagnet $\alpha-Cu_2V_2O_7$, *Phys. Rev. B* **92**, 024423 (2015).
- [69] G. Gitgeatpong, Y. Zhao, P. Piyawongwatthana, Y. Qiu, L. W. Harriger, N. P. Butch, T. J. Sato, and K. Matan, Nonreciprocal Magnons and Symmetry-Breaking in the Noncentrosymmetric Antiferromagnet, *Phys. Rev. Lett.* **119**, 047201 (2017).
- [70] D. Hirai, T. Yajima, K. Nawa, M. Kawamura, and Z. Hiroi, Anisotropic triangular lattice realized in rhenium oxychlorides $A_3ReO_5Cl_2$ ($A = Ba, Sr$), *Inorg. Chem.* **59**, 10025 (2020).